ACS OMEGA

http://pubs.acs.org/journal/acsodf

Article

P176S Mutation Rewires Electrostatic Interactions That Alter Maspin Functionality

Muhammad Ayaz Anwar, Muhammad Haseeb, Sangdun Choi, and Kwang Pyo Kim*

Cite This: *ACS Omega* 2023, 8, 28258−28267

Read Online

ACCESS | Metrics & More | Article Recommendations | Supporting Information

ABSTRACT: Maspin is known to regress tumors by inhibiting angiogenesis; however, its roles have been reported to be context- and sequence-dependent. Various proteins and cofactors bind to maspin, possibly explaining its conflicting roles. Moreover, polymorphic forms of maspin have also been linked to tumor regression and survival; for instance, maspin with Ser at 176 (maspin-S176) promotes tumors, while maspin with Pro at 176 (maspin-P176) has opposing roles in cancer pathogenesis. With the help of long molecular dynamics simulations, a possible link between polymorphic forms and tumor progression has been established. First, maspin is dynamically stable with either amino acid at the 176 position. Second, differential contacts have been observed among various regions; third, these contacts have significantly altered the electrostatic energetics of various residues; finally, these altered electrostatics of maspin-S176 and maspin-P176 rewire the polar contacts that abolished the allosteric control of the protein. By combining these factors, the altered electrostatics substantially affect the localization and preference of maspin-binding partners, thus culminating in a different maspin-protein(cofactor)-interaction landscape that may have been manifested in previous conflicting reports. Here, the underlying reason has been highlighted and discussed, which may be helpful for better therapeutic manipulation.

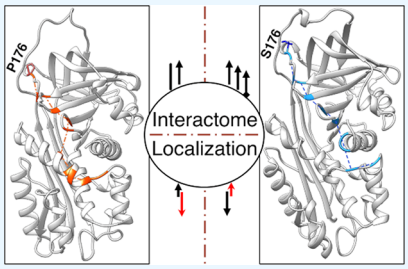

1. INTRODUCTION

Cancer growth can be prevented by multiple antitumor proteins that, if activated during the early phase, trigger apoptosis and hinder the accumulation of transformed cells. Despite the large number of antitumor proteins, the prevalence of cancer is increasing, and further studies are needed to rationalize the tumor initiation mechanism. Among the known factors for cancers, inactivation of antitumor proteins, over-activation of protumor proteins, and evasion of immune surveillance are notable. Once the tumor mass has been established, cells invade and metastasize to other tissues, a phenomenon known as epithelial-mesenchymal transition (EMT). This process has been executed by different transcription factors, such as Snail, Slug, Twist, and Zeb1/2, during embryogenesis and in malignant tumor cells in various combinations.[1−4] EMT can be characterized by the loss of adherens junctions and changes in cell morphology from a polygonal/epithelial to a spindly/fibroblastic shape, increased motility, activation of matrix-degrading enzymes, and resistance to apoptosis. For instance, E-cadherin is a direct target of various transcription factors that can deprive tumor cells of this key suppressor of motility and invasiveness.[5]

Among the several tumor suppressors genes, maspin is a class II tumor suppressor protein that stimulates apoptosis and suppresses motility, invasion, and metastasis and was first identified in 1994.[6,7] Maspin is a non-inhibitory serpin and is more closely related to clade B serpins owing to its reactive site loop (RCL) that is shorter than those of inhibitory serpins. Unlike multiple other serpins, maspin does not undergo a stressed-relaxed conformational change to inhibit protease activity. Despite the lack of protease inhibition, recent studies provide evidence for its ability to regulate cell adhesion, motility, apoptosis, and angiogenesis, making it an attractive target for various forms of malignancies.[8−11]

Maspin expression has been reported in various cancers, including gastric cancer,[12−14] and its reactivation can suppress breast tumors in xenograft models.[15] It has been proposed as a biomarker of colorectal cancer,[16] lung cancer,[17] oral cancer,[18] and cervical lesions.[19] The expression of maspin has been evaluated in a wide range of cancers and found to be over- or under-expressed depending on the type of cancer. Three coding region polymorphic forms of maspin have been reported, among which P176S (reference SNP cluster ID; rs2289519) is linked to the promotion of gastric cancer[20] and V187L (rs2289520) is linked to oral cancer.[21] Maspin-P176, in conjunction with maspin-L187, decreases the risk of esophageal squamous cell carcinoma, whereas maspin-S176 (with maspin-V187) exerts the opposite effect.[22] Additionally, the homozygous maspin-S176 has been linked with gallbladder cancer.[23] However, how a minor variation in the unstructured

Received: March 19, 2023
Accepted: June 21, 2023
Published: July 26, 2023

region can drastically alter the function of an antitumor protein to protumor protein is still a mystery.

Structural biology has advanced our understanding of the three-dimensional structures of different proteins; however, the lack of a dynamic picture of these proteins hinders their functional aspects. The detailed analysis and resolution offered by molecular dynamics simulations (MDS) bridge the gap between structural biology and the dynamic nature of proteins.[24] In this study, we analyzed proteomics data from 80 early onset gastric cancers and found that maspin was overexpressed in most of the samples. Furthermore, long MDS were performed for two polymorphic forms, maspin-P176 and maspin-S176, and extensive energetics analysis was carried out. It was observed that although the residual contacts are altered to a small scale, the per-residue and paired-residue energetics are significantly perturbed. The rearrangement of the polar network and disturbance of allosteric signals are evident, which makes maspin with small structural differences interact with different partners and result in opposing effects.

2. MATERIALS AND METHODS

2.1. Maspin Modeling. The three-dimensional coordinates for the maspin protein were downloaded from the RCSB Protein Data Bank [PDB ID:1WZ9, higher resolution (2.1 Å) but lacks the loop region],[25] and the missing loop residues (amino acids 331−342) were built using the Swiss-Model online webserver.[26] After construction of the model, it was compared with 1XQG (low-resolution 3.1 Å but complete),[27] and the loop was in agreement with the crystal structure. As the protein structure was of moderate quality, the hydrogen atoms have been added based on the force-field definition, and most of the His residues are ε-protonated (in the HIE state), while H320, H352, and H360 are δ-protonated (in the HID state). For maspin-P176, the serine was mutated in Chimera v1.1.3[28] using the Dunbrack 2010[29] rotamer library with subsequent 500 steps of steepest descent energy minimization with a 0.002 Å step size and an update of 100 conjugate gradient of the same step size with none of the atoms fixed during minimization.

2.2. MD Simulations. All MDS were performed in GROMACS v2019.6[30] using the AMBER99SB-ILDN force field[31] with a dodecahedron box filled with the rigid TIP3P water model.[32] Periodic boundary conditions were applied in all directions. The system was neutralized, and the NaCl concentration was adjusted to 0.1 M (48 Na^+, 41 Cl^-). The system was energy-minimized to 500 kJ/mol/nm using the steepest descent algorithm, and two-step equilibrations were performed. Initially, the temperature was adjusted to 310 K for 1 ns using the V-Rescale method[33] with 0.1 ps time constant, and isotropic pressure (1 bar and 2.0 ps time constant) was then applied to the system following the Parrinello−Rahman algorithm.[34] During equilibration, position restraints were applied to avoid structural distortions. Particle mesh Ewald[35] was used to treat long-range electrostatic interactions with cubic interpolation, and a 10 Å cutoff was used for short-range Coulomb and van der Waals interactions. For each system, five independent production simulations were performed for a length of 1 μs starting from a different random seed with only bonds involving hydrogen atom constraints using the Library of Integrated Network-Based Cellular Signatures (LINCS),[36] and a trajectory snapshot was saved at 10 ps. Therefore, a total of 10 μs simulation was conducted, and most of the analysis was conducted for the last 500 ns with a 100 ps gap, making a total of 25,000 snapshots for each analysis.

2.3. Calculation of Nonbonded Interaction Energies. The residual and paired-residue nonbonded interaction energies were calculated between maspin-P176 and maspin-S176 as follows; the differential residual average nonbonded energy of residue i is

$$\Delta E_i = E_i^{\text{Maspin}-\text{P176}} - E_i^{\text{Maspin}-\text{S176}}$$

where ΔE_i refers to the change in nonbonded interaction energy between residue "i" of maspin-P176 ($E_i^{\text{Maspin-P176}}$) and maspin-S176 ($E_i^{\text{Maspin-S176}}$). The differential residual average nonbonded energy of residue "i" with water is as follows:

$$\Delta E_i^{\text{water}} = \langle E_i^{\text{water,Maspin}-\text{P176}} \rangle - \langle E_i^{\text{water,Maspin}-\text{S176}} \rangle$$

Here, the $\langle E_i^{\text{water,Maspin-P176}} \rangle$ indicates the average contribution of nonbonded energy from water toward the residue "i" for each indicated system. The paired-residue interaction energies for residues i and j in maspin-P176 and maspin-S176 were calculated as follows:

$$\Delta E_{ij} = \langle \Delta E_{ij}^{\text{Maspin}-\text{P176}} \rangle - \langle \Delta E_{ij}^{\text{Maspin}-\text{S176}} \rangle$$

The symbols $\langle\rangle$ indicate the ensemble average for the respective energy terms[electrostatic (E^{Elect}) and van der Waals (Vdw, E^{Vdw})] between the residues "i" and "j"; however, the Vdw energy terms are negligible compared to electrostatic interactions. Therefore, primarily E^{Elect} has been discussed in detail.

2.4. Differential Contact Map. The contact between two residues was defined as the distance between heavy atoms less than 4.5 Å with four residues apart.[37] The contacts were calculated for the last 500 ns of each trajectory (total frames of 25,000), and the interatomic contact fraction was defined as $f_{ij} = n_{ij}/N$, where n_{ij} is the number of frame contacts between atom_i and atom_j and N is the total number of frames. However, for the residue, the individual contacts were summed; thus, a value of more than 1 is possible.

2.5. Allosteric Coupling Intensity Analysis. The allostery among the residues was calculated using Ohm, which employs the concept of perturbation propagation to determine the allostery in proteins.[38] Because the allosteric communications depend on the interatomic contacts, a contact distance of 4.5 Å was used, with the probability of perturbation from one residue to another set to 0.05 and the number of perturbation rounds set to 10,000. The value of α was set to 0.5 to capture the possible allosteric probability. The remaining parameters were maintained at default values, as provided by the algorithm.

2.6. Analysis. Most of the analyses were performed using tools provided with GROMACS v2019.6 and the Amber trajectory processing tool (CPPTRAJ).[39] The 3D protein figures were generated using Chimera v1.1.3, and plots were generated using MS Excel and the Matplotlib library.[40]

2.7. Statistical Test. For the statistical test, the data were binned into 25 sets, and an average of each set was then used to assess the significance (p-value < 0.05) using a two-tailed Student's t test in SciPy with default parameters.[41]

3. RESULTS

3.1. Maspin Is Stable during MD Simulation. From the gastric cancer dataset of 80 patients, maspin was upregulated in 55 (69%) and downregulated in 8 (10%), while it was not

https://doi.org/10.1021/acsomega.3c01850
ACS Omega 2023, 8, 28258−28267

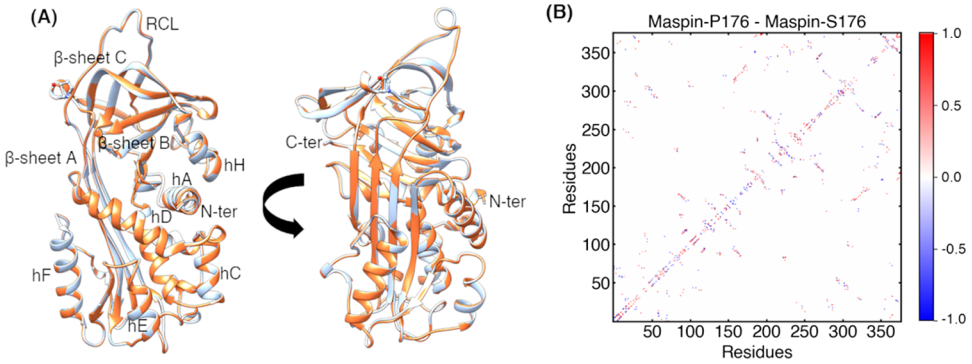

Figure 1. Structure and contact analysis of maspin. (A) 3D structure of maspin (P176 is represented in light blue and S176 in brown). The prominent secondary structural elements are also labeled. (B) Differential contact map analysis of maspin-P176 and maspin-S176 from the energy-minimized structures. C/N-ter, C/N terminal; RCL, reactive center loop.

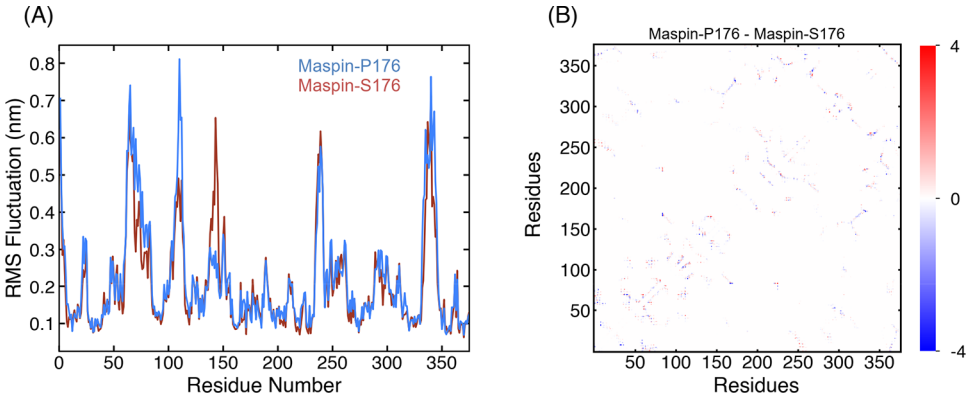

Figure 2. RMSF and differential contact frequency map. (A) Average RMSF for both systems for the last 500 ns of each trajectory. (B) Contacts among heavy atoms only have been calculated with a cutoff of 4.5 Å and contacts measured for only residues with 4 residues apart. The maximum fractional change was found to be 6.4; however, for matrix representation, the color was anchored at 4 for better visualization, as only 0.39% contacts are beyond this range.

detected/significant in 17 (21%) samples (Figure S1). Normally, maspin-P176 acts as a tumor suppressor; however, the substitution of P176S can alter its functions, making it a protumor protein, prompting this study to reveal the functional aspects of these polymorphic forms (Figure 1A). From protein modeling, both forms are nearly identical [the root-mean-square deviation (RMSD) between Cα is 0.16 Å over 375 atom pairs while 0.37 Å over 5916 atom pairs excluding the 176th position as the number of atoms is different between Pro and Ser]; however, substantial differences were noted in the analysis of the inter-residue contacts (Figure 1B), indicating side-chain rearrangements in maspin-S176 and maspin-P176. Therefore, to further study the impact of side-chain rearrangement, each polymorphic form, i.e., maspin-P176 and maspin-S176, was subjected to five independent 1 μs long all-atom MDS.

As the polymorphic forms differed in a single amino acid (Ser or Pro at 176) in a loop region, none of the proteins underwent any conformational change (Figure S2). After the initial adjustment for approximately 300 ns (the RMSD change was approximately 0.25 nm), the RMSD of each protein remained stable for the remaining simulation length (approximately 0.1 nm) (Figure S2A). Other structural measures, such as solvent-accessible surface area (SASA), were also consistent (Figure S2B). The average number of intra-protein hydrogen bonds was higher in maspin-S176 (290.4 vs 286.4 in maspin-P176); however, the total number of hydrogen bonds was substantially lower than that of the crystal structure (i.e., 412).[25] The hydrogen bonds between the protein and water were not significantly different (Student's t test p-value = 0.6) (Figure S2C,D), indicating that internal reordering of the bonding network is plausible.

The number of water molecules in the first and second shells around maspin-P176 (1379.3 ± 25 and 2200 ± 34.5) and maspin-S176 (1370.9 ± 26 and 2191.1 ± 38.3) is in a close range. Similarly, the fraction of native contacts (Q) indicated that the proteins were in an intermediate-active state, preserving approximately 0.43 of the native contacts in both cases (Figure S2E).[42] It has been shown that these proteins can fold to a metastable conformation before folding into a stable conformation, which assists in their functions. Moreover, maspin-S176 exhibited a lower packing density with a higher number of cavities, indicating that it is less compact (Figure S3A,B).

Recently, maspin residues 87 to 114 have been proposed to harbor nuclear localization signals, and their exposure impacts maspin localization.[43] When the exposure was calculated for the entire length, maspin-S176 showed slightly higher solvent accessibility than maspin-P176. However, solvent exposure for maspin-S176 was significantly higher for 87−94 (s2A; 2nd strand in β-sheet A), referring to the higher possibility of this variant being nuclear-localized (Figure S4).

3.2. Differential Contact Map Highlights the Pivotal Difference in P176S. Despite the conformational stability,

https://doi.org/10.1021/acsomega.3c01850
ACS Omega 2023, 8, 28258−28267

the per-residue fluctuation is different between maspin-P176 and maspin-S176. As per root-mean-square fluctuation (RMSF), most of the residues fluctuated proportionally to each other; however, the non-structured region showed higher fluctuations, such as residues 61−83 (loop between hC-hD and hD), 102−113 (hE and proceeding loop), the loop between hF and s3A (138−150; s3A refers to the 3rd strand of β-sheet A), the loop between s3B and hG (234−242), and the prominent RCL region 334−345 (Figure 2A). These fluctuations can initiate inter-residue signaling that could influence the dynamic behavior of the protein.

Next, the residue contact map was analyzed as the residue communication occurs through residual contacts that exert influence over neighboring residues. Due to the dynamic nature of proteins, these contacts are formed and break dynamically over time. This provides an intuitive way to analyze the close collaboration and allosteric influence of various residues. In Figure 2B, the blue and red dots represent the higher fraction of contacts in maspin-S176 and maspin-P176, respectively, with a maximum change of approximately 30% in contact frequency (Table S1). The change in contact and close proximity refer to the rewiring of contacts and allosteric communication. For instance, the difference in contact between residues S40-F70 (−27.2, hB-hD, can influence collagen binding), K268-H344 (−24.8, influences RCL mobility), Y84-K170 (−23.1, helps expose Y84 and phosphorylation), M172-S333 (−19.7, in the vicinity of the mutated site and base of RCL), and Y84-F167 (−18.3, influences hydrophobic packing) was increased in maspin-S176, whereas Y84-H225 (29.9, protects the shutter region), E218−F229 (28.9, β-sheet B, core hydrophobic region), F60−F70 (23.6 hC and hD, may alter collagen binding), E289−K294 (19.8, solvent-accessible), and T241-P353 (17.1, influences hG movement) were decreased. Similarly, the base of the RCL showed substantial contact with the region around 176 in maspin-S176, highlighting the mobile side-chain interactions.

3.3. Rewiring of Electrostatic Interactions Is Evident in P176S. As it is evident that there are alterations in inter-residue contacts and all nonbonded interactions arise from these contacts, it is reasonable to argue that the nonbonded interactions have also been perturbed (Figure 3). The nonbonded interaction energies [electrostatic (E^{Elect}) and Vdw (E^{Vdw})] were calculated for each residue and between the protein and water. The total nonbonded interaction energy ($E^{Total} = E^{Elect} + E^{Vdw}$ and $\langle \Delta E^{Total} \rangle = \langle$Maspin-P176$^{Elect + Vdw}\rangle$ - $\langle$Maspin-S176$^{Elect + Vdw}\rangle$) is heavily influenced by the change in electrostatic energy, whereas ΔE^{Vdw} is nominal (mostly <2 kcal/mol). Because ΔE^{Total} is proportional to ΔE^{Elect}, it is rational to focus on ΔE^{Elect}.

The residues with significantly perturbed electrostatic energy were scattered across the protein, including the mutated position 176 (15.98 kcal/mol). In Figure 3, positive and negative values indicate favorable and unfavorable ΔE^{Elect}, respectively, in maspin-S176. Among these residues, E61 (−43.2 kcal/mol) and K64 (−48.7 kcal/mol) showed the highest unfavorable energy for maspin-S176 and are present on the hC−hD loop, far from the mutation site. Moreover, E335, E340, and E347 are present on or around the RCL, whereas E335, which is closer to residue 176, can participate in altering the dynamics of the RCL. R91, K109, and R110 are part of the positive residue clusters that severely alter their ΔE^{Elect}, which is known to bind cofactors and proteins in many maspins.[43−45]

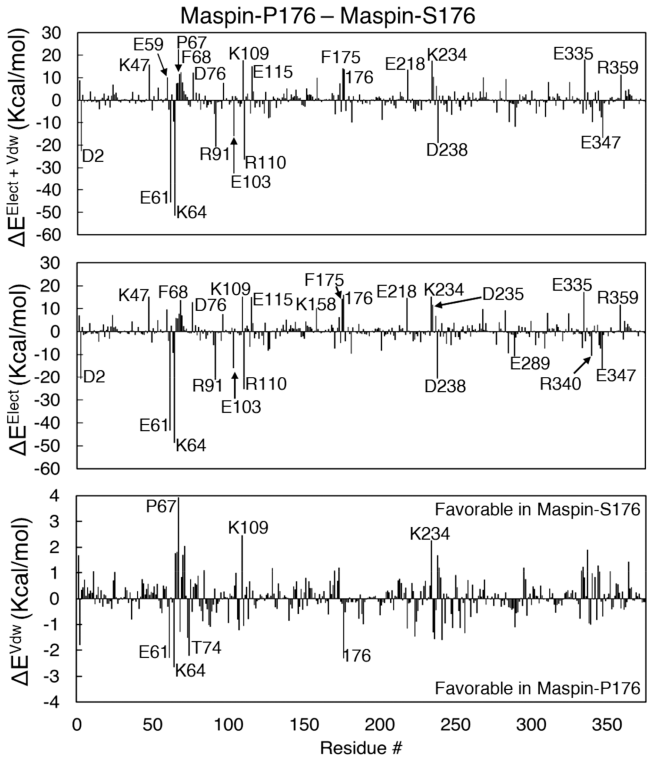

Figure 3. Per-residue energy perturbation in maspin. The average energy change has been calculated from 5000 snapshots of each trajectory. The total interaction energy is the sum of nonbonded electrostatic and van der Waals energy terms.

Here, only R91 has unfavorable electrostatic energy in maspin-S176. ΔE^{Elect} in this region is also critical as it acts as a nuclear localization signal and altered electrostatic interactions can mask or unmask this region.[43] E218 and R359 are located on β-sheet B, which could significantly alter the inter-residue distance and compactness of the protein (Figure S3). Similarly, the overall distance between the acidic (D and E) and basic residues (K, R, and H) is significantly higher in maspin-S176 (Student's t test $p < 0.01$, 95% CI in mean; −0.202 to −0.212, Figure S5), indicating that electrostatic energies can alter the physical state of the protein. Concerning the ΔE^{Vdw} interaction energies, P67, K109, and K234 showed favorable ΔE^{Vdw} in maspin-S176, while E61, K64, T74, and S176 showed unfavorable ΔE^{Vdw} in maspin-S176.

The residual interaction energy between protein residues and water was also dominated by ΔE^{Elect}. Most of the residues are polar and show favorable ΔE^{Elect} in maspin-S176 with water, which is rational and provides solvent-mediated dipole orientation to fine-tune protein solubility and functions.[46] In the case of the ΔE^{Vdw}, only Y112 and S176 are prominent (Figure S6). Y112, with a phenol side chain, can be phosphorylated, resulting in altered functions.

3.4. Propagation of Electrostatic Perturbation in P176S Maspin. As it is now known that mutation causes significant changes in electrostatic interactions, it is important to know how these perturbations travel across the protein. For this, the pairwise residue interaction ($\Delta E_{ij}^{Elect} = \langle E_{ij} \rangle^{P176} - \langle E_{ij} \rangle^{S176}$) was calculated for all interacting pairs (Figure 4, Figure S7; the numerical values of $|\Delta E_{ij}| > 4$ kcal/mol are given in Table S2). The interacting residues were drawn as a network to visualize how the signal traveled from the mutated site (Figure 5).

https://doi.org/10.1021/acsomega.3c01850
ACS Omega 2023, 8, 28258−28267

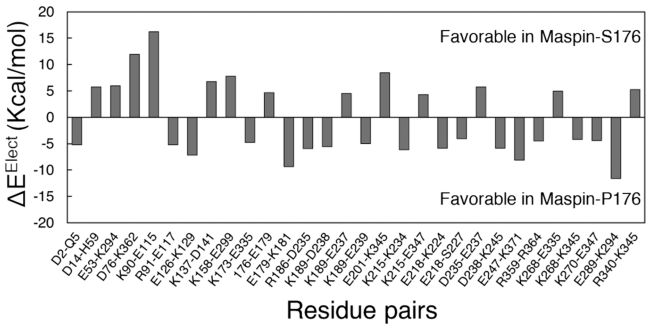

Figure 4. Pair residue ΔE^{Elect} interaction energy. The ΔE^{Elect} is substantial between P176 and S176 (only residue pairs with > ±4 kcal/mol are shown).

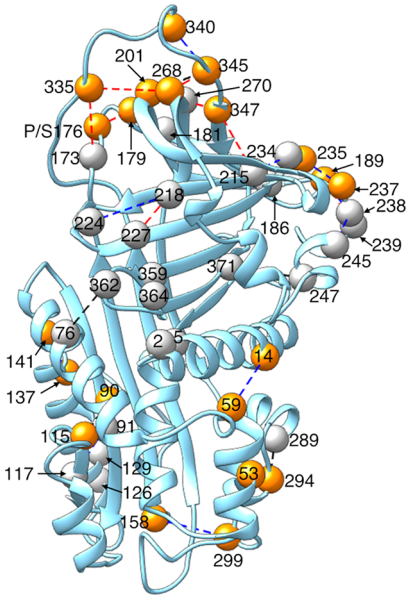

Figure 5. Network view of paired-residue interaction energy. The network view of the paired-residue ΔE^{Elect} interaction energy with only residue pair with > ± 4 kcal/mol is shown. The black dotted lines represent $|\Delta E^{\text{Elect}}| > 10$ kcal/mol, blue denotes the $|\Delta E^{\text{Elect}}| > 6$ kcal/mol, and red denotes $|\Delta E^{\text{Elect}}| > 4$ kcal/mol. The residues with favorable interactions in maspin-S176 are represented in orange, while those with unfavorable interactions are represented in gray.

The paired residue-wise electrostatic interaction energies were substantially different for various residue pairs. For instance, D14-H59 (5.7 kcal/mol) and K90-E115 (16.2 kcal/mol) form salt bridges, and it is seen that both show favorable electrostatic interactions in maspin-S176. These pairs are far from the mutation site; however, they display a substantial electrostatic influence. Moreover, salt-bridge formation between K90-E115 and D14-H59 is energetically expansive and generally destabilizes the protein structure. Such electrostatic interactions can play a role in determining the specificity of various protein-mediated interactions.[47−49] Similarly, E201-K345 (8.4 kcal/mol) displayed a favorable interaction that may assist the RCL terminal region to get the anchor. The effect of mutation was unfavorable in its vicinity, E179-K181 (−9.3 kcal/mol), where a polar substitution (P176S) might create charge repulsion. Comparably, E289-K294 (−11.6 kcal/mol) and E247-K371 (−8.1 kcal/mol) also exhibit the unfavorable interactions.

The mutation from Pro to Ser causes a local electrostatic disruption that triggers perturbation of neighboring residues, such as 173, 179, and E201. Residue 173 interacts with residue 335 (the base of RCL), which then propagates the signal through β-sheet C and RCL to the stretch of residues ranging from K234, D235, E237 D238, and E239, which can alter the electrostatic potential (Figure 5). Similarly, hG is in close proximity that has been reported to move, resulting in an open conformation in the crystallographic structure. It has been implicated in collagen binding, altering the overall kinetics of protein−protein interactions and acting as a conformational switch.[25] Moreover, E218 is in s2B, which can significantly change the inner core potential and alter the interaction between the T259-R364 residue pair, which is directly connected to hA. From β-sheet A, only a few residues, such as K90, R91, D115, and E117, are affected, indicating that the inter-residue ΔE^{Elect} alteration can propagate the signal to a longer distance.

Concerning the Vdw interaction energy, only a small stretch of protein exhibits drastic changes; for example, D351-H352 was highly stable in maspin-S176, while H352-P353 was stable in maspin-P176 (Figure S7). These residue positions were in close proximity to the mutation site, which could cause the polar or nonpolar energetic differences to be the highest. Similarly, H360 showed substantial stability with T363 and D76. Moreover, N163-H320 was buried in the core, which was also more stable in maspin-S176.

3.5. P176S Substitution Alters the Ionic Bonding Network. The substitution of P176S causes significant alteration in electrostatic interactions, and since almost all of these residues are polar, they are capable of forming ionic bonds (salt bridges and hydrogen bonds) with each other. Consequently, it is intuitive to evaluate the frequency of ionic interactions between the residues. The representative polar contacts are shown in Figure 6. It should be noted that these contacts are dynamic and can exist in different forms in different conformations.

In Figure 7, the probability distribution of the minimum distance of the side chains and the differential hydrogen bond (HB) frequencies ($\text{Hbond}^{\text{P176}}-\text{Hbond}^{\text{S176}}$) are shown. The overall pattern is similar for most of the pairs, albeit the intensity varies; thus, the HB frequencies (negative values indicate the higher presence of HB in maspin-S176). For instance, the residue pairs K90-E115, D14-H59, E247-K371, E289-K294, and K158-E299 exhibit a strong single peak at 0.2 nm that indicates ionic interaction (salt bridge or HB). K90-E115, D14-H59, and K158-E299 were more stable in maspin-S176, whereas E247-K371 (hG and s5B) and E289-K294 (hH and proceeding loop) were unstable. D76-K362, E201-K345, and D238-K245 all showed two or more peaks, with D76-K362 and E201-K345 being more stable in maspin-S176. There is a single pair that has a non-overlapping population shift, D235-E237, with maspin-P176 having a stable interaction and higher HB propensity than maspin-S176. Finally, no hydrogen bond was found between R340 and K345 mainly due to the disordered nature of RCL. These population shifts of polar ionic bonds can change the inter-residue distance, electrostatic interactions, allosteric signaling and communication, and continuity of charges that significantly modulate the protein binding mode.

Salt bridge formation between K90-E115 and D14-H59 has been reported in a crystal structure with Ser at position 176;[25] however, in the case of P176, these salt bridges were

https://doi.org/10.1021/acsomega.3c01850
ACS Omega 2023, 8, 28258−28267

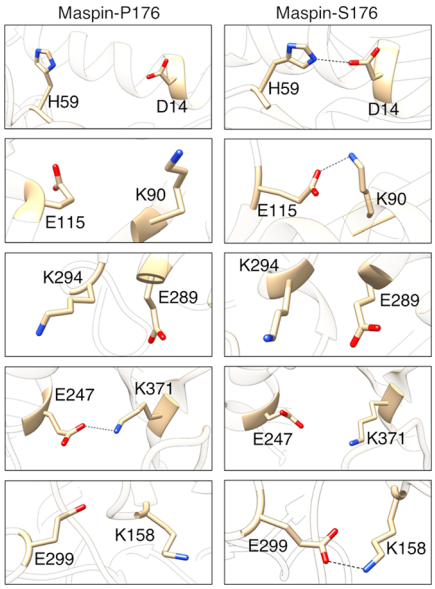

Figure 6. Representative snapshots of residues with polar contacts. These contacts are dynamic and represent ensemble average. The contacting residues are in stick representation with heteroatoms colored, and hydrogen is hidden for clarity. The remaining protein is made transparent to highlight the contacting residues.

dramatically reduced. This indicates that the electrostatic interactions can have a ripple effect. Moreover, it can be inferred that the stronger polar interactions between these residues should stabilize the protein, as has already been reported for various thermophiles.[50]

3.6. P176S Causes the Loss of Allosteric Coordination in Maspin. Mutation caused the electrostatic interactions and bonding network to shift dramatically, and the next question is whether these rearrangements can have any impact on allosteric interactions within proteins. As allostery is pivotal in protein functioning, improper signaling can heavily influence functional capability.

The mutation P176S caused a dramatic decrease in allosteric coupling intensity (ACI, a measure of the allosteric influence from one residue to another) (Figure 8A, numerical values with $|\Delta ACI| > 600$ are provided in Table S3).[38] In the case of maspin-S176, almost all the residues showed a substantial drop in ACI values. The reduction is prominent for residues 175, 185, 186, 197, 198, 204, 206, 271, 273, and 353, where the $\Delta ACI > 200$. Most of these residues were located in the vicinity of the mutation. The pathways followed by signal propagation had lower weights in maspin-S176 than in maspin-P176, and the paths were mostly similar (Figure 8B,C, Table S4). The signaling path is only divergent from residue 360; in maspin-P176, it mostly goes to residue 363, whereas in maspin-S176, residue 365 is the prominent candidate. From 363/365, different routes were followed to reach the target residue (K64).

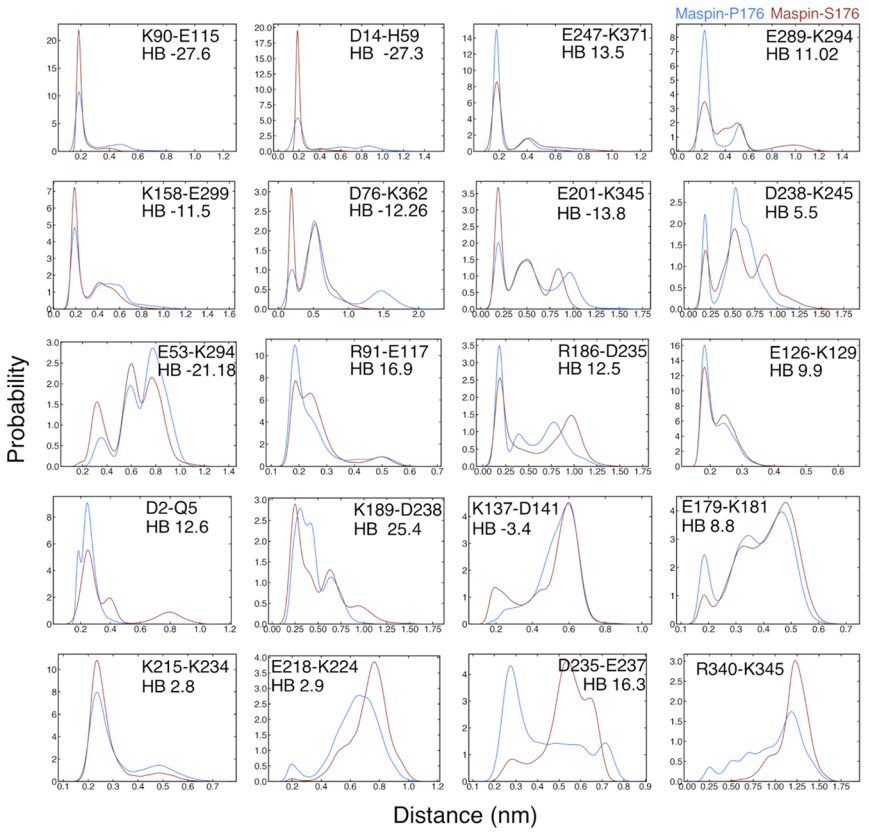

Figure 7. Paired residue distance distribution and hydrogen bond occupancy. The minimum distance between residue pairs has been calculated for the last 5000 snapshots of each trajectory and plotted as the distribution graph for only pairs with $|\Delta E^{Elect}| > 5$ kcal/mol. The change in HB occupancy (maspin-P176^{HB}−maspin-S176^{HB}) has been given as well (except R340-K345 as only single HB was observed). The presence of polar contacts such as salt-bridge or HB can be analyzed by the peak at 0.2 nm.

https://doi.org/10.1021/acsomega.3c01850
ACS Omega 2023, 8, 28258−28267

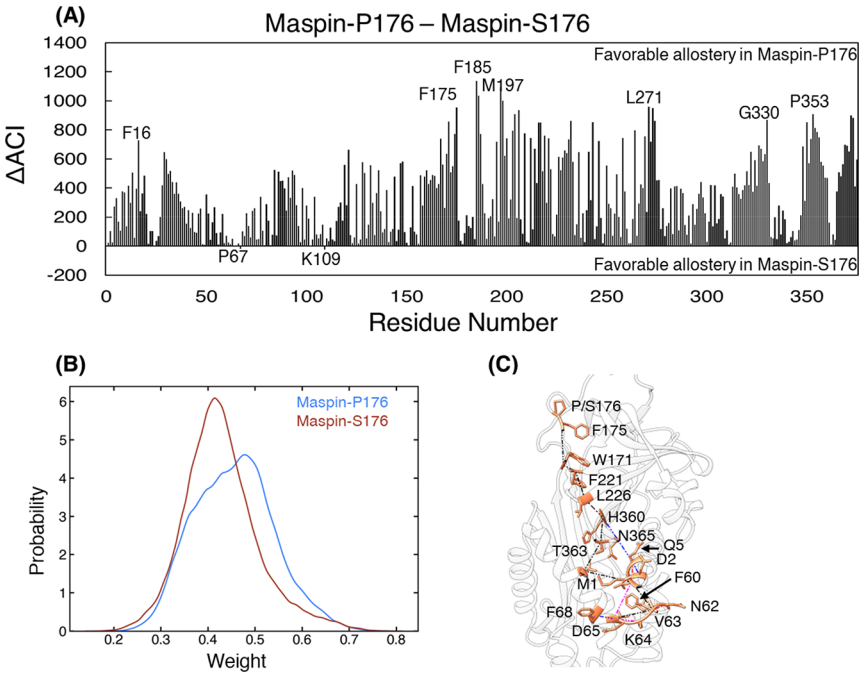

Figure 8. Allosteric coupling intensity (ACI). (A) ACI values have been calculated using a perturbation propagation algorithm that analyzes the probability of propagating the signal from the allosteric site (in this case, 176th residue) to the target site (here 64 chosen as the active residue as it shows the highest ΔE^{Elect}). The residues with positive values represent decrease, while residues with negative values represent increase in ACI in maspin-S176. Few residues have been labeled for reference. (B) Distribution of weights from the highest probable paths from the allosteric site to the target site using 25,000 snapshots (Kolmogorov–Smirnov p-value $\ll 0.001$). (C) Prominent pathways connecting the residues are shown. The path indicated by black dotted lines is common among all the paths, while the remaining color scheme is given in Table S4 along with the residue numbers and frequency of frames where the given path has been identified.

4. DISCUSSION

The purpose of this study was to identify the critical elements that govern the differential role of maspins in spatiotemporal contexts using long-unbiased MDS. In MDS, the non-inhibitory maspin is stable and in an active state conformation that exhibits inter-residue and paired-residue electrostatic perturbation in response to mutation. These electrostatic perturbations reduce the allosteric coupling within the protein, altering the entire maspin-interaction landscape and resulting in altered interacting partner preference,[51] cellular localization and stability,[52,53] and posttranslational modification propensity (as reviewed in refs 54, 55). To further explore the protein–protein interactions (molecular docking simulations) that consider the significant changes in electrostatic interactions, further studies are required.

The localization and cellular environment of maspin largely dictate its pro- or antitumor functions.[56−61] Recently, it has been reported that maspin can translocate to the nucleus by active and passive mechanisms, and it also harbors nuclear localization signals spanning from 87 to 114 (s2A and hE).[43] This region holds a strong salt bridge, K90-E115, in maspin, which can help mask/unmask this region and regulate nuclear localization. In our analysis, maspin-S176 was slightly more exposed (Figure S4A,B), which should favor nuclear localization; however, for antitumor activity, more than one variable may be involved. Furthermore, maspin cellular localization is regulated by cellular confluency and epidermal growth factor receptor-related pathways, implicating their role in maspin function.[62] Nuclear-localized maspin inhibits breast cancer proliferation.[13] Similarly, Dzinic et al. reported that nuclear-localized maspin effectively inhibits HDAC1 functions and suppresses the growth of multiple cancer cell lines, including lung and prostate, and that nuclear localization is favored by mutations around the RCL region (maspin-D346E).[59] Both these residues are negatively charged and should not alter the isoelectric point; however, a longer side chain of glutamate could offer more interacting opportunities.

Maspin interacts with various proteins, including interferon regulatory factor 6,[63] type I and III collagen,[64] urokinase-type plasminogen activator and its receptor,[65] β1-integrin,[66] heparin,[44] heat shock protein (HSP) 70, HSP90, glutathione S-transferase,[67] and Bax (an apoptosis-related protein).[68] Electrostatic interactions have been shown to play a role in ternary complex formation in the transcriptional adaptor zinc-binding domain 1 protein, illustrating vital electrostatic control in protein binding and localization.[69] Furthermore, in maspin-S176, the favorable $\Delta E_{ij}^{\text{Elect}}$ interaction increased for surface residues that could modulate solvent interaction and hence stability and alter the binding partner preference (Figure 5, Table S2).[52] In addition, the altered charge distribution in proteins attracts new partners such as fatty acid-binding protein 5 (FABP5), which forces the basic residues to align and create a docking site for importin binding that subsequently translocates FABP5 to the nucleus.[70] In maspin, a similar alignment can be achieved by altering the inter-residue interactions.[43]

In maspin, residues from hD, hE, and hG form a negative patch that binds with collagen, an integral cellular component that is critical for angiogenesis, sharing a similar binding interface with other serpin family members such as pigment epithelium-derived factors.[25,64,71] Among these residues, E61 and D238 exhibit unfavorable ΔE^{Elect} and hG harboring electrostatically repulsive pairs that may substantially affect collagen binding (Figures 5 and 6). Similarly, RCL has been

https://doi.org/10.1021/acsomega.3c01850
ACS Omega 2023, 8, 28258−28267

reported to promote cell adhesion,[59,61] and mutations in this region may hamper its activity. Due to its solvent-exposed and disordered nature, there were a few residues with significantly perturbed energetics, such as E335, R340, and possibly E347. The mutation of R340 is suggestive of loss of cell adhesion, and R340 exhibits unfavorable ΔE^{Elect} whose energy is partly compensated by interacting with K345 in maspin-S176. Therefore, altered electrostatics may hamper interactions with other proteins and cofactors (Figures 5 and 6).

Allosteric regulation is known to regulate a variety of protein functions such as protein binding,[72] and complex formation,[73] and single nucleotide polymorphisms (SNPs) affect allostery[74] and allosteric polymorphism. The role of these mutations has been extensively studied in tailored medicine;[75,76] however, classifying P176S as a cancer driver requires further study.

In conclusion, the P176S mutation in maspin altered residual electrostatic energetics and created an altered paired-residue interaction pattern. These altered electrostatic charges can substantially change the binding partner preference, mode, localization, and stability, which can influence the overall functions of the protein in the cellular environment.

■ ASSOCIATED CONTENT

Data Availability Statement

All the softwares used in this study are freely available. The trajectories of protein simulation can be obtained from the corresponding author upon reasonable request.

Supporting Information

The Supporting Information is available free of charge at https://pubs.acs.org/doi/10.1021/acsomega.3c01850.

Additional experimental details, methods, and results, including photographs of the experimental setup (PDF)

■ AUTHOR INFORMATION

Corresponding Author

Kwang Pyo Kim − *Department of Applied Chemistry, Institute of Natural Science, Global Center for Pharmaceutical Ingredient Materials, Kyung Hee University, Yongin 17104, Republic of Korea; Department of Biomedical Science and Technology, Kyung Hee Medical Science Research Institute, Kyung Hee University, Seoul 02447, Republic of Korea;* orcid.org/0000-0003-0095-3787; Email: kimkp@khu.ac.kr

Authors

Muhammad Ayaz Anwar − *Department of Applied Chemistry, Institute of Natural Science, Global Center for Pharmaceutical Ingredient Materials, Kyung Hee University, Yongin 17104, Republic of Korea;* orcid.org/0000-0002-8794-5589

Muhammad Haseeb − *Department of Molecular Science and Technology, Ajou University, Suwon 16499, Republic of Korea;* orcid.org/0000-0003-1224-8276

Sangdun Choi − *Department of Molecular Science and Technology, Ajou University, Suwon 16499, Republic of Korea;* orcid.org/0000-0001-5920-7848

Complete contact information is available at: https://pubs.acs.org/10.1021/acsomega.3c01850

Author Contributions

M.A.A. and K.P.K. designed the study, K.P.K. arranged the materials, M.A.A., M.H., and S.C. conducted simulations, and M.A.A. and K.P.K. analyzed the results and wrote the draft. All authors read and approved the final draft of the manuscript.

Notes

The authors declare no competing financial interest.

■ ACKNOWLEDGMENTS

This work was supported by the National Research Foundation of Korea grant (NRF-2019M3E5D3073567).

■ REFERENCES

(1) Micalizzi, D. S.; Farabaugh, S. M.; Ford, H. L. Epithelial-Mesenchymal Transition in Cancer: Parallels between Normal Development and Tumor Progression. *J. Mammary Gland Biol. Neoplasia* **2010**, *15*, 117−134.

(2) Schmalhofer, O.; Brabletz, S.; Brabletz, T. E-Cadherin, Beta-Catenin, and ZEB1 in Malignant Progression of Cancer. *Cancer Metastasis Rev.* **2009**, *28*, 151−166.

(3) Yang, J.; Weinberg, R. A. Epithelial-Mesenchymal Transition: At the Crossroads of Development and Tumor Metastasis. *Dev. Cell* **2008**, *14*, 818−829.

(4) Taube, J. H.; Herschkowitz, J. I.; Komurov, K.; Zhou, A. Y.; Gupta, S.; Yang, J.; Hartwell, K.; Onder, T. T.; Gupta, P. B.; Evans, K. W.; Hollier, B. G.; Ram, P. T.; Lander, E. S.; Rosen, J. M.; Weinberg, R. A.; Mani, S. A. Core Epithelial-to-Mesenchymal Transition Interactome Gene-Expression Signature Is Associated with Claudin-Low and Metaplastic Breast Cancer Subtypes. *Proc. Natl. Acad. Sci. U. S. A.* **2010**, *107*, 15449−15454.

(5) Peinado, H.; Marin, F.; Cubillo, E.; Stark, H.-J.; Fusenig, N.; Nieto, M. A.; Cano, A. Snail and E47 Repressors of E-Cadherin Induce Distinct Invasive and Angiogenic Properties in Vivo. *J. Cell Sci.* **2004**, *117*, 2827−2839.

(6) Khalkhali-Ellis, Z. Maspin: The New Frontier. *Clin. Cancer Res.* **2006**, *12*, 7279−7283.

(7) Zou, Z.; Anisowicz, A.; Hendrix, M. J.; Thor, A.; Neveu, M.; Sheng, S.; Rafidi, K.; Seftor, E.; Sager, R. Maspin, a Serpin with Tumor-Suppressing Activity in Human Mammary Epithelial Cells. *Science* **1994**, *263*, 526−529.

(8) Berardi, R.; Morgese, F.; Onofri, A.; Mazzanti, P.; Pistelli, M.; Ballatore, Z.; Savini, A.; De Lisa, M.; Caramanti, M.; Rinaldi, S.; Pagliaretta, S.; Santoni, M.; Pierantoni, C.; Cascinu, S. Role of Maspin in Cancer. *Clin. Transl. Med.* **2013**, *2*, 8.

(9) McGowen, R.; Biliran, H.; Sager, R.; Sheng, S. The Surface of Prostate Carcinoma DU145 Cells Mediates the Inhibition of Urokinase-Type Plasminogen Activator by Maspin. *Cancer Res.* **2000**, *60*, 4771−4778.

(10) Schaefer, J. S.; Zhang, M. Role of Maspin in Tumor Metastasis and Angiogenesis. *Curr. Mol. Med.* **2003**, *3*, 653−658.

(11) Sheng, S.; Truong, B.; Fredrickson, D.; Wu, R.; Pardee, A. B.; Sager, R. Tissue-Type Plasminogen Activator Is a Target of the Tumor Suppressor Gene Maspin. *Proc. Natl. Acad. Sci. U. S. A.* **1998**, *95*, 499−504.

(12) Kim, S. M.; Cho, S. J.; Jang, W. Y.; Kim, D. H.; Shin, H. S.; Jang, M. K.; Kim, H. Y.; Nam, E. S. Expression of Maspin Is Associated with the Intestinal Type of Gastric Adenocarcinoma. *Cancer Res. Treat.* **2005**, *37*, 228−232.

(13) Tanaka, A.; Wang, J. Y.; Shia, J.; Zhou, Y.; Ogawa, M.; Hendrickson, R. C.; Klimstra, D. S.; Roehrl, M. H. A. Maspin as a Prognostic Marker for Early Stage Colorectal Cancer With Microsatellite Instability. *Front. Oncol.* **2020**, *10*, 945.

(14) Zheng, H.-C.; Gong, B.-C. The Roles of Maspin Expression in Gastric Cancer: A Meta- and Bioinformatics Analysis. *Oncotarget* **2017**, *8*, 66476−66490.

(15) Beltran, A.; Parikh, S.; Liu, Y.; Cuevas, B. D.; Johnson, G. L.; Futscher, B. W.; Blancafort, P. Re-Activation of a Dormant Tumor Suppressor Gene Maspin by Designed Transcription Factors. *Oncogene* **2007**, *26*, 2791−2798.

(16) Banias, L.; Gurzu, S.; Kovacs, Z.; Bara, T.; Bara, T.; Jung, I. Nuclear Maspin Expression: A Biomarker for Budding Assessment in

Colorectal Cancer Specimens. *Pathol., Res., Pract.* **2017**, *213*, 1227−1230.
(17) Berardi, R.; Morgese, F.; Savini, A.; Onofri, A.; Cascinu, S. Maspin Staining and Its Use as Biomarker in Lung Cancer. In *Biomarkers in Cancer*; Preedy, V. R., Patel, V. B., Eds.; Biomarkers in Disease: Methods, Discoveries and Applications; Springer Netherlands: Dordrecht, 2015; p 345−358.
(18) Shpitzer, T.; Hamzany, Y.; Bahar, G.; Feinmesser, R.; Savulescu, D.; Borovoi, I.; Gavish, M.; Nagler, R. M. Salivary Analysis of Oral Cancer Biomarkers. *Br. J. Cancer* **2009**, *101*, 1194−1198.
(19) Manawapat-Klopfer, A.; Thomsen, L. T.; Martus, P.; Munk, C.; Russ, R.; Gmuender, H.; Frederiksen, K.; Haedicke-Jarboui, J.; Stubenrauch, F.; Kjaer, S. K.; Iftner, T. TMEM45A, SERPINB5 and P16INK4A Transcript Levels Are Predictive for Development of High-Grade Cervical Lesions. *Am. J. Cancer Res.* **2016**, *6*, 1524−1536.
(20) Jang, H.-L.; Nam, E.; Lee, K. H.; Yeom, S.; Son, H. J.; Park, C. Maspin Polymorphism Associated with Apoptosis Susceptibility and in Vivo Tumorigenesis. *Int. J. Mol. Med.* **2008**, *22*, 333−338.
(21) Yang, P.-Y.; Miao, N.-F.; Lin, C.-W.; Chou, Y.-E.; Yang, S.-F.; Huang, H.-C.; Chang, H.-J.; Tsai, H.-T. Impact of Maspin Polymorphism Rs2289520 G/C and Its Interaction with Gene to Gene, Alcohol Consumption Increase Susceptibility to Oral Cancer Occurrence. *PLoS One* **2016**, *11*, No. e0160841.
(22) Meng, H.; Guan, X.; Guo, H.; Xiong, G.; Yang, K.; Wang, K.; Bai, Y. Association between SNPs in Serpin Gene Family and Risk of Esophageal Squamous Cell Carcinoma. *Tumour Biol.* **2015**, *36*, 6231−6238.
(23) Mahananda, B.; Vinay, J.; Palo, A.; Singh, A.; Sahu, S. K.; Singh, S. P.; Dixit, M. SERPINB5 Genetic Variants Rs2289519 and Rs2289521 Are Significantly Associated with Gallbladder Cancer Risk. *DNA Cell Biol.* **2021**, *40*, 706−712.
(24) Hollingsworth, S. A.; Dror, R. O. Molecular Dynamics Simulation for All. *Neuron* **2018**, *99*, 1129−1143.
(25) Law, R. H. P.; Irving, J. A.; Buckle, A. M.; Ruzyla, K.; Buzza, M.; Bashtannyk-Puhalovich, T. A.; Beddoe, T. C.; Nguyen, K.; Worrall, D. M.; Bottomley, S. P.; Bird, P. I.; Rossjohn, J.; Whisstock, J. C. The High Resolution Crystal Structure of the Human Tumor Suppressor Maspin Reveals a Novel Conformational Switch in the G-Helix. *J. Biol. Chem.* **2005**, *280*, 22356−22364.
(26) Waterhouse, A.; Bertoni, M.; Bienert, S.; Studer, G.; Tauriello, G.; Gumienny, R.; Heer, F. T.; de Beer, T. A. P.; Rempfer, C.; Bordoli, L.; Lepore, R.; Schwede, T. SWISS-MODEL: Homology Modelling of Protein Structures and Complexes. *Nucleic Acids Res.* **2018**, *46*, W296−W303.
(27) Al-Ayyoubi, M.; Gettins, P. G. W.; Volz, K. Crystal Structure of Human Maspin, a Serpin with Antitumor Properties: Reactive Center Loop of Maspin Is Exposed but Constrained. *J. Biol. Chem.* **2004**, *279*, 55540−55544.
(28) Pettersen, E. F.; Goddard, T. D.; Huang, C. C.; Couch, G. S.; Greenblatt, D. M.; Meng, E. C.; Ferrin, T. E. UCSF Chimera?A Visualization System for Exploratory Research and Analysis. *J. Comput. Chem.* **2004**, *25*, 1605−1612.
(29) Shapovalov, M. V.; Dunbrack, R. L. A Smoothed Backbone-Dependent Rotamer Library for Proteins Derived from Adaptive Kernel Density Estimates and Regressions. *Structure* **2011**, *19*, 844−858.
(30) Abraham, M. J.; Murtola, T.; Schulz, R.; Páll, S.; Smith, J. C.; Hess, B.; Lindahl, E. GROMACS: High Performance Molecular Simulations through Multi-Level Parallelism from Laptops to Supercomputers. *SoftwareX* **2015**, *1−2*, 19−25.
(31) Lindorff-Larsen, K.; Piana, S.; Palmo, K.; Maragakis, P.; Klepeis, J. L.; Dror, R. O.; Shaw, D. E. Improved Side-Chain Torsion Potentials for the Amber Ff99SB Protein Force Field: Improved Protein Side-Chain Potentials. *Proteins: Struct., Funct., Bioinf.* **2010**, *78*, 1950−1958.
(32) Jorgensen, W. L.; Chandrasekhar, J.; Madura, J. D.; Impey, R. W.; Klein, M. L. Comparison of Simple Potential Functions for Simulating Liquid Water. *J. Chem. Phys.* **1983**, *79*, 926−935.
(33) Bussi, G.; Donadio, D.; Parrinello, M. Canonical Sampling through Velocity Rescaling. *J. Chem. Phys.* **2007**, *126*, No. 014101.
(34) Parrinello, M.; Rahman, A. Polymorphic Transitions in Single Crystals: A New Molecular Dynamics Method. *J. Appl. Phys.* **1981**, *52*, 7182−7190.
(35) Darden, T.; York, D.; Pedersen, L. Particle Mesh Ewald: An N·log(N) Method for Ewald Sums in Large Systems. *J. Chem. Phys.* **1993**, *98*, 10089−10092.
(36) Hess, B.; Bekker, H.; Berendsen, H. J. C.; Fraaije, J. G. E. M. LINCS: A Linear Constraint Solver for Molecular Simulations. *J. Comput. Chem.* **1997**, *18*, 1463−1472.
(37) Yuan, C.; Chen, H.; Kihara, D. Effective Inter-Residue Contact Definitions for Accurate Protein Fold Recognition. *BMC Bioinf.* **2012**, *13*, 292.
(38) Wang, J.; Jain, A.; McDonald, L. R.; Gambogi, C.; Lee, A. L.; Dokholyan, N. V. Mapping Allosteric Communications within Individual Proteins. *Nat. Commun.* **2020**, *11*, 3862.
(39) Roe, D. R.; Cheatham, T. E. PTRAJ and CPPTRAJ: Software for Processing and Analysis of Molecular Dynamics Trajectory Data. *J. Chem. Theory Comput.* **2013**, *9*, 3084−3095.
(40) Hunter, J. D. Matplotlib: A 2D Graphics Environment. *Comput. Sci. Eng.* **2007**, *9*, 90−95.
(41) Virtanen, P.; Gommers, R.; Oliphant, T. E.; Haberland, M.; Reddy, T.; Cournapeau, D.; Burovski, E.; Peterson, P.; Weckesser, W.; Bright, J.; van der Walt, S. J.; Brett, M.; Wilson, J.; Millman, K. J.; Mayorov, N.; Nelson, A. R. J.; Jones, E.; Kern, R.; Larson, E.; Carey, C. J.; Polat, İ.; Feng, Y.; Moore, E. W.; VanderPlas, J.; Laxalde, D.; Perktold, J.; Cimrman, R.; Henriksen, I.; Quintero, E. A.; Harris, C. R.; Archibald, A. M.; Ribeiro, A. H.; Pedregosa, F.; Van Mulbregt, P.; SciPy 1.0 Contributors; Vijaykumar, A.; Bardelli, A. P.; Rothberg, A.; Hilboll, A.; Kloeckner, A.; Scopatz, A.; Lee, A.; Rokem, A.; Woods, C. N.; Fulton, C.; Masson, C.; Häggström, C.; Fitzgerald, C.; Nicholson, D. A.; Hagen, D. R.; Pasechnik, D. V.; Olivetti, E.; Martin, E.; Wieser, E.; Silva, F.; Lenders, F.; Wilhelm, F.; Young, G.; Price, G. A.; Ingold, G.-L.; Allen, G. E.; Lee, G. R.; Audren, H.; Probst, I.; Dietrich, J. P.; Silterra, J.; Webber, J. T.; Slavič, J.; Nothman, J.; Buchner, J.; Kulick, J.; Schönberger, J. L.; De Miranda Cardoso, J. V.; Reimer, J.; Harrington, J.; Rodríguez, J. L. C.; Nunez-Iglesias, J.; Kuczynski, J.; Tritz, K.; Thoma, M.; Newville, M.; Kümmerer, M.; Bolingbroke, M.; Tartre, M.; Pak, M.; Smith, N. J.; Nowaczyk, N.; Shebanov, N.; Pavlyk, O.; Brodtkorb, P. A.; Lee, P.; McGibbon, R. T.; Feldbauer, R.; Lewis, S.; Tygier, S.; Sievert, S.; Vigna, S.; Peterson, S.; More, S.; Pudlik, T.; Oshima, T.; Pingel, T. J.; Robitaille, T. P.; Spura, T.; Jones, T. R.; Cera, T.; Leslie, T.; Zito, T.; Krauss, T.; Upadhyay, U.; Halchenko, Y. O.; Vázquez-Baeza, Y. SciPy 1.0: Fundamental Algorithms for Scientific Computing in Python. *Nat. Methods* **2020**, *17*, 261−272.
(42) Giri Rao, V. V. H.; Gosavi, S. On the Folding of a Structurally Complex Protein to Its Metastable Active State. *Proc. Natl. Acad. Sci. U. S. A.* **2018**, *115*, 1998−2003.
(43) Reina, J.; Zhou, L.; Fontes, M. R. M.; Panté, N.; Cella, N. Identification of a Putative Nuclear Localization Signal in the Tumor Suppressor Maspin Sheds Light on Its Nuclear Import Regulation. *FEBS Open Bio* **2019**, *9*, 1174−1183.
(44) Sheng, S.; Carey, J.; Seftor, E. A.; Dias, L.; Hendrix, M. J.; Sager, R. Maspin Acts at the Cell Membrane to Inhibit Invasion and Motility of Mammary and Prostatic Cancer Cells. *Proc. Natl. Acad. Sci. U. S. A.* **1996**, *93*, 11669−11674.
(45) Parker, M. W.; Rossjohn, J.; Cappai, R.; Feil, S. C.; Henry, A.; McKinstry, W. J.; Galatis, D.; Hesse, L.; Multhaup, G.; Beyreuther, K.; Masters, C. L. No Title Found. *Nat. Struct. Biol.* **1999**, *6*, 327−331.
(46) Qiao, B.; Jiménez-Ángeles, F.; Nguyen, T. D.; Olvera de la Cruz, M. Water Follows Polar and Nonpolar Protein Surface Domains. *Proc. Natl. Acad. Sci. U. S. A.* **2019**, *116*, 19274−19281.
(47) Hendsch, Z. S.; Tidor, B. Do Salt Bridges Stabilize Proteins? A Continuum Electrostatic Analysis: Salt-Bridge Effects on Protein Stability. *Protein Sci.* **1994**, *3*, 211−226.
(48) Nakamura, H. Roles of Electrostatic Interaction in Proteins. *Q. Rev. Biophys.* **1996**, *29*, 1−90.

https://doi.org/10.1021/acsomega.3c01850
ACS Omega 2023, 8, 28258−28267

(49) Zhou, H.-X.; Pang, X. Electrostatic Interactions in Protein Structure, Folding, Binding, and Condensation. *Chem. Rev.* **2018**, *118*, 1691−1741.
(50) Kumar, S.; Nussinov, R. How Do Thermophilic Proteins Deal with Heat? *Cell. Mol. Life Sci.* **2001**, *58*, 1216−1233.
(51) Zhang, Z.; Witham, S.; Alexov, E. On the Role of Electrostatics in Protein−Protein Interactions. *Phys. Biol.* **2011**, *8*, No. 035001.
(52) Strickler, S. S.; Gribenko, A. V.; Gribenko, A. V.; Keiffer, T. R.; Tomlinson, J.; Reihle, T.; Loladze, V. V.; Makhatadze, G. I. Protein Stability and Surface Electrostatics: A Charged Relationship. *Biochemistry* **2006**, *45*, 2761−2766.
(53) Kudriaeva, A.; Kuzina, E. S.; Zubenko, O.; Smirnov, I. V.; Belogurov, A., Jr. Charge-Mediated Proteasome Targeting. *FASEB J.* **2019**, *33*, 6852−6866.
(54) Bianchi, G.; Longhi, S.; Grandori, R.; Brocca, S. Relevance of Electrostatic Charges in Compactness, Aggregation, and Phase Separation of Intrinsically Disordered Proteins. *Int. J. Mol. Sci.* **2020**, *21*, 6208.
(55) Vascon, F.; Gasparotto, M.; Giacomello, M.; Cendron, L.; Bergantino, E.; Filippini, F.; Righetto, I. Protein Electrostatics: From Computational and Structural Analysis to Discovery of Functional Fingerprints and Biotechnological Design. *Comput. Struct. Biotechnol. J.* **2020**, *18*, 1774−1789.
(56) Bernardo, M. M.; Kaplun, A.; Dzinic, S. H.; Li, X.; Irish, J.; Mujagic, A.; Jakupovic, B.; Back, J. B.; Van Buren, E.; Han, X.; Dean, I.; Chen, Y. Q.; Heath, E.; Sakr, W.; Sheng, S. Maspin Expression in Prostate Tumor Cells Averts Stemness and Stratifies Drug Sensitivity. *Cancer Res.* **2015**, *75*, 3970−3979.
(57) Dzinic, S. H.; Bernardo, M. M.; Li, X.; Fernandez-Valdivia, R.; Ho, Y.-S.; Mi, Q.-S.; Bandyopadhyay, S.; Lonardo, F.; Vranic, S.; Oliveira, D. S. M.; Bonfil, R. D.; Dyson, G.; Chen, K.; Omerovic, A.; Sheng, X.; Han, X.; Wu, D.; Bi, X.; Cabaravdic, D.; Jakupovic, U.; Wahba, M.; Pang, A.; Harajli, D.; Sakr, W. A.; Sheng, S. An Essential Role of *Maspin* in Embryogenesis and Tumor Suppression. *Cancer Res.* **2017**, *77*, 886−896.
(58) Sakabe, T.; Wakahara, M.; Shiota, G.; Umekita, Y. Role of Cytoplasmic Localization of Maspin in Promoting Cell Invasion in Breast Cancer with Aggressive Phenotype. *Sci. Rep.* **2021**, *11*, 11321.
(59) Dzinic, S. H.; Kaplun, A.; Li, X.; Bernardo, M.; Meng, Y.; Dean, I.; Krass, D.; Stemmer, P.; Shin, N.; Lonardo, F.; Sheng, S. Identification of an Intrinsic Determinant Critical for Maspin Subcellular Localization and Function. *PLoS One* **2013**, *8*, No. e74502.
(60) Zhang, M.; Volpert, O.; Shi, Y. H.; Bouck, N. Maspin Is an Angiogenesis Inhibitor. *Nat. Med.* **2000**, *6*, 196−199.
(61) Ngamkitidechakul, C.; Warejcka, D. J.; Burke, J. M.; O'Brien, W. J.; Twining, S. S. Sufficiency of the Reactive Site Loop of Maspin for Induction of Cell-Matrix Adhesion and Inhibition of Cell Invasion. *J. Biol. Chem.* **2003**, *278*, 31796−31806.
(62) Longhi, M. T.; Silva, L. E.; Pereira, M.; Magalhães, M.; Reina, J.; Vitorino, F. N. L.; Gumbiner, B. M.; da Cunha, J. P. C.; Cella, N. PI3K-AKT, JAK2-STAT3 Pathways and Cell−Cell Contact Regulate Maspin Subcellular Localization. *Cell Commun. Signal.* **2021**, *19*, 86.
(63) Bailey, C. M.; Khalkhali-Ellis, Z.; Kondo, S.; Margaryan, N. V.; Seftor, R. E. B.; Wheaton, W. W.; Amir, S.; Pins, M. R.; Schutte, B. C.; Hendrix, M. J. C. Mammary Serine Protease Inhibitor (Maspin) Binds Directly to Interferon Regulatory Factor 6: IDENTIFICATION OF A NOVEL SERPIN PARTNERSHIP*[Boxs]. *J. Biol. Chem.* **2005**, *280*, 34210−34217.
(64) Blacque, O. E.; Worrall, D. M. Evidence for a Direct Interaction between the Tumor Suppressor Serpin, Maspin, and Types I and III Collagen. *J. Biol. Chem.* **2002**, *277*, 10783−10788.
(65) Pemberton, P. A.; Tipton, A. R.; Pavloff, N.; Smith, J.; Erickson, J. R.; Mouchabeck, Z. M.; Kiefer, M. C. Maspin Is an Intracellular Serpin That Partitions into Secretory Vesicles and Is Present at the Cell Surface. *J. Histochem. Cytochem.* **1997**, *45*, 1697−1706.
(66) Cella, N.; Contreras, A.; Latha, K.; Rosen, J. M.; Zhang, M.; Cella, N.; Contreras, A.; Latha, K.; Rosen, J. M.; Zhang, M. Maspin Is Physically Associated with B1 Integrin Regulating Cell Adhesion in Mammary Epithelial Cells. *FASEB J.* **2006**, *20*, 1510−1512.
(67) Yin, S.; Li, X.; Meng, Y.; Finley, R. L.; Sakr, W.; Yang, H.; Reddy, N.; Sheng, S. Tumor-Suppressive Maspin Regulates Cell Response to Oxidative Stress by Direct Interaction with Glutathione S-Transferase. *J. Biol. Chem.* **2005**, *280*, 34985−34996.
(68) Liu, J.; Yin, S.; Reddy, N.; Spencer, C.; Sheng, S. Bax Mediates the Apoptosis-Sensitizing Effect of Maspin. *Cancer Res.* **2004**, *64*, 1703−1711.
(69) Wang, Y.; Brooks, C. L., III Electrostatic Forces Control the Negative Allosteric Regulation in a Disordered Protein Switch. *J. Phys. Chem. Lett.* **2020**, *11*, 864−868.
(70) Armstrong, E. H.; Goswami, D.; Griffin, P. R.; Noy, N.; Ortlund, E. A. Structural Basis for Ligand Regulation of the Fatty Acid-Binding Protein 5, Peroxisome Proliferator-Activated Receptor β/δ (FABP5-PPARβ/δ) Signaling Pathway. *J. Biol. Chem.* **2014**, *289*, 14941−14954.
(71) Meyer, C.; Notari, L.; Becerra, S. P. Mapping the Type I Collagen-Binding Site on Pigment Epithelium-Derived Factor. *J. Biol. Chem.* **2002**, *277*, 45400−45407.
(72) Lin, S. L.; Xu, D.; Li, A.; Nussinov, R. Electrostatics, Allostery, and Activity of the Yeast Chorismate Mutase. *Proteins: Struct., Funct., Genet.* **1998**, *31*, 445−452.
(73) Soisson, S. M.; MacDougall-Shackleton, B.; Schleif, R.; Wolberger, C. Structural Basis for Ligand-Regulated Oligomerization of AraC. *Science* **1997**, *276*, 421−425.
(74) Tee, W.-V.; Guarnera, E.; Berezovsky, I. N. On the Allosteric Effect of NsSNPs and the Emerging Importance of Allosteric Polymorphism. *J. Mol. Biol.* **2019**, *431*, 3933−3942.
(75) Nussinov, R.; Tsai, C.-J. 'Latent Drivers' Expand the Cancer Mutational Landscape. *Curr. Opin. Struct. Biol.* **2015**, *32*, 25−32.
(76) Nussinov, R.; Jang, H.; Tsai, C.-J.; Cheng, F. Correction: Review: Precision Medicine and Driver Mutations: Computational Methods, Functional Assays and Conformational Principles for Interpreting Cancer Drivers. *PLoS Comput. Biol.* **2019**, *15*, No. e1007114.

https://doi.org/10.1021/acsomega.3c01850
ACS Omega 2023, 8, 28258−28267